Eur. Phys. J. B **19**, 215–223 (2001)

THE EUROPEAN PHYSICAL JOURNAL B

EDP Sciences

Evolution of $(La_{1-y}Pr_y)_{0.7}Ca_{0.3}MnO_3$ crystal structure with A-cation size, temperature, and oxygen isotope substitution

A.M. Balagurov[1], V.Yu. Pomjakushin[1,2], D.V. Sheptyakov[1,a], V.L. Aksenov[1], N.A. Babushkina[3], L.M. Belova[3], O.Yu. Gorbenko[4], and A.R. Kaul[4]

[1] Frank Laboratory of Neutron Physics, JINR, 141980, Dubna, Russia
[2] Laboratory for Neutron Scattering ETHZ & PSI, 5232 Villigen PSI, Switzerland
[3] RRC "Kurchatov Institute", Kurchatov sq. 1, 123182, Moscow, Russia
[4] Chemistry Department, Moscow State University, 119899, Moscow, Russia

Received 28 April 2000

Abstract. The atomic structure of $(La_{1-y}Pr_y)_{0.7}Ca_{0.3}MnO_3$ compound with $0.5 \leq y \leq 1$ has been systematically studied by neutron powder diffraction in the temperature range from 15 to 293 K. For composition with $y = 0.75$, the structural analysis was performed on two samples, one containing the natural mixture of oxygen isotopes and the other one 75% enriched by ^{18}O. The room temperature structural characteristics of the series, including cell volume, average Mn-O bond distance, and average Mn-O-Mn bond angle, are the linear functions of the $\langle r_A \rangle$. Temperature dependencies of these parameters are quite smooth, except for the point $T = T_{FM}$, where a jump like changes occur. The isotope enriched samples have been found identical in crystal and magnetic structure down to the temperature of transition of the sample with ^{16}O into the metallic ferromagnetic phase. It confirms that different transport and magnetic properties of the samples with ^{16}O and ^{18}O at low temperature are driven by the different oxygen atoms dynamics solely. Temperature dependencies of the CO and AFM diffraction peak intensities and of the peak widths for compositions close to the metal-insulator boundary ($y \approx 0.75$) indicate the macroscopically phase separated AFM-dielectric + FM-metallic state below T_{FM}.

PACS. 75.30.Vn Colossal magnetoresistance – 61.12.Ld Single-crystal and powder diffraction

1 Introduction

Intensive investigations of CMR-manganites with the general formula $A_{1-x}A'_xMnO_3$ (where A is La or other rare-earth element, A′ is the alkali-earth divalent ion like Ca, Sr) during last few years have persuasively demonstrated that their transport (electric conductivity), magnetic (low-temperature magnetic ordering type) and structural (the lattice symmetry, the degree of the oxygen octahedra distortions) properties are closely correlated to each other, and for the revelation of the full physical essence it is necessary to study them in parallel. Besides, it was also shown that the particular attention is needed to the investigation of the coupling between the electron and phonon subsystems in manganites. Several papers have already been published, where this coupling was convincingly demonstrated by the substitution of oxygen ^{16}O by ^{18}O. In particular the change in the oxygen mass leads to the significant lowering of the Curie temperature (for example, by 21 K after 95% substitution of ^{16}O by ^{18}O in $La_{0.8}Ca_{0.2}MnO_3$ [1]), or even to the total suppression of the transition to the metallic state (as in $(La_{0.5}Nd_{0.5})_{0.67}Ca_{0.33}MnO_3$ [2] and $(La_{0.25}Pr_{0.75})_{0.7}Ca_{0.3}MnO_3$ [3]).

The certain properties of CMR-compounds depend mainly on the amount of the divalent cation (the doping level), x, and, on the average ionic radius, $\langle r_A \rangle$, of the cations situating in the A-position of the perovskite structure [4]. For the given doping level, the change in the phase state may be done by successive substitution of rare-earth cations, *i.e.* by changing $\langle r_A \rangle$. The compound $(La_{1-y}Pr_y)_{0.7}Ca_{0.3}MnO_3$ (LPCM-Z, where $Z = 100 \times y$, hereafter), the structural neutron-diffraction investigation of which is presented in this paper, is in this sense indicative, because the change of y from 0 to 1 leads to the considerable change in the low-temperature magnetic state: for $y = 0$ ($\langle r_A \rangle \approx 1.21$ Å) it is ferromagnetic metal ($T_{FM} \approx 250$ K) [5], and for $y = 1$ ($\langle r_A \rangle \approx 1.18$ Å) it is an insulator with the complicated magnetic structure [6–8].

The phase diagram for the $A_{1-x}A'_xMnO_3$ compositions with $x = 0.3$ (Ref. [9]) shows that $\langle r_A \rangle \approx 1.19$ Å(corresponding to the tolerance factor of perovskite-like structure $t \approx 0.91$) is a critical value separating the metallic and the insulating states. It has been shown in references [3,10], that the LPCM composition with $y = 0.75$,

[a] e-mail: Denis.Sheptyakov@psi.ch

for which $\langle r_A \rangle = 1.186$ Å, becomes essentially sensitive to the different physical effects, so that even the isotope substitution of ^{16}O by ^{18}O causes the change of the low-temperature state from metallic to insulating. A possible microscopic model of such transition was discussed in reference [10] in terms of the isotope dependence of the effective electron bandwidth in the proximity of the insulator-metal phase boundary. For checking and refining the theoretical models, the information on the atomic and magnetic structure as a function of $\langle r_A \rangle$ at a constant doping level is essential. In this case, the changes in transport properties might be related to the conduction bandwidth, which is, in turn, related to the values of the valence angles Mn-O-Mn, as it was shown, for example, in reference [9].

In our previous neutron-diffraction papers on the compositions $(La_{1-y}Pr_y)_{0.7}Ca_{0.3}MnO_3$ with $y = 0.5$ [11] and $y = 0.75$ [12], we mainly studied their magnetic properties. It was shown that the low-temperature magnetic structure correlates with the behaviour of the electric resistivity. In particular, it was found that two samples of the compound with $y = 0.75$ (one of which contained the natural isotope mixture (99.7% ^{16}O) and was metallic at $T \leq 110$ K, and the other was 75% – enriched by ^{18}O isotope and remained insulating down to helium temperatures), do possess different magnetic structures. The observed temperature dependencies of the diffraction peaks intensities in LPCM with $y = 0.75$ [12] turned out to be qualitatively the same as for the $(La_{0.5}Nd_{0.5})_{0.67}Ca_{0.33}MnO_3$ composition, two samples of which, enriched with the ^{16}O and ^{18}O isotopes, were investigated by Ibarra *et al.* with neutron diffraction [13]. In that study, it was shown that in the sample with ^{16}O, the FM contribution to the nuclear peaks intensities is high, and the intensity of the superstructural AFM peaks is low, while in the sample with ^{18}O, the situation is opposite. The authors of reference [13] concluded that the strong electron-phonon interaction is present, which influences the observed effects, and suggested the existence of the two electronically segregated phases in the sample with ^{16}O.

In the papers of Millis *et al.* [14,15], the possible scenario for the charge delocalization in CMR compounds was substantiated, in which the distortions of the oxygen octahedra around the Mn^{+3} cations, which exist in the paramagnetic insulating phase and promote the localization of charges in the form of "Jahn-Teller polarons", disappear at the transition to the FM phase. The first indication for such a mechanism was already obtained in the classic paper of Wollan and Koehler [16], and in the latest time – in some diffraction experiments (see, for example, Refs. [11,17,18]). These data and especially the experiments with oxygen isotope enriched samples confirm the importance of the electron-phonon coupling for the physics of the CMR-manganites, but nevertheless no proves of structural identity of the isotope enriched samples in the above mentioned papers were granted till now. As a result, the papers have appeared (see, *e.g.*, Ref. [19]), which propose non-phonon mechanisms for the isotope effect in CMR.

In this paper, we present the systematic structural data for the $(La_{1-y}Pr_y)_{0.7}Ca_{0.3}MnO_3$ series as functions of temperature. One of the main goals of this work was the precise study of crystal structure of two samples with $y = 0.75$ with different contents of the ^{16}O and ^{18}O oxygen isotopes. We show that the samples are structurally identical in the temperature interval between room temperature and the temperature of the ^{16}O sample transition to the metallic ferromagnetic phase, $T_{FM,O\text{-}16}$ and, consequently, their essentially different transport and magnetic properties at $T < T_{FM,O\text{-}16}$ are determined only by the differences in the oxygen atoms dynamics. Also, the evidences are presented for existence of spatially separated (onto the antiferro- and ferromagnetic phases) state in the ^{16}O sample with $y = 0.75$.

2 Samples preparation and neutron diffraction experiments

Several samples of $(La_{1-y}Pr_y)_{0.7}Ca_{0.3}MnO_3$ with $0.5 \leq y \leq 1$ were prepared as powders with the use of the so-called "paper synthesis". For this, an aqueous solution of a mixture of La, Pr, Ca, and Mn nitrates taken in the required ratios was soaked by ash-free paper filters, which were dried (120 °C) and then burnt. The oxide product thus obtained was annealed in air at 700 °C for 2 h. The final thermal treatment consisted of annealing the pressed pellets in air at 1200 °C for 12 h. The process of the $(La_{0.25}Pr_{0.75})_{0.7}Ca_{0.3}MnO_3$ composition enrichment by the oxygen isotopes was carried out at $T = 950$ °C and $p = 1$ atm. Two samples were treated simultaneously: one was heated in natural $^{16}O_2$ atmosphere (99.7 % enrichment), the other one was heated in $^{18}O_2$ atmosphere (85% enrichment). The powder was placed in the platinum boats situated in two parallel quartz tubes. Each tube was a part of the closed circuit. In one circuit, the $^{16}O_2$ oxygen circulated, in the other – the ^{18}O isotope enriched gaz. 11 sequential changes of the oxygen atmosphere in the circuit were done. The impoverished due to the exchange oxygen gas was removed, and the circuit was refilled with the "fresh" oxygen $^{18}O_2$ with the 85% isotope enrichment. The whole time of annealing at 950 °C was 100 h. The final ^{18}O oxygen content in the O-18 sample was about 75%. It was determined from the weight changing and mass-spectroscopy analysis of oxygen atmosphere in the contour. Hereafter, these samples with $y = 0.75$ and oxygen ^{16}O and ^{18}O isotopes are referred to as O-16 and O-18, correspondingly.

The mass of the samples prepared for the neutron-diffraction experiments was about 5 g each. For all the samples, the temperature dependencies of the resistivity and magnetic susceptibility were measured. Their low-temperature magnetic structure was defined in neutron-diffraction experiments, carried out with the DMC diffractometer in the Paul Scherrer Institute at SINQ neutron source. The results of these investigations will be published elsewhere. The main characteristics of the samples studied are given in Table 1.

Table 1. Some characteristics of the $(La_{1-y}Pr_y)_{0.7}Ca_{0.3}MnO_3$ compounds. The samples investigated in the present paper, are marked as LPCM-50, and so on. For the compositions with $y = 0$, 0.25 and 1, the data from the literature are given. The values of $\langle r_A \rangle$ are calculated with the use of the values tabulated in [24] for the 9-fold coordination. The tolerance factor was calculated as $t = (1/\sqrt{2})(\langle r_A \rangle + r_O)/(\langle r_{Mn} \rangle + r_O)$, where $r_O = 1.32$ Å and $\langle r_{Mn} \rangle = 0.62$ Å. T_{FM} is the temperature of the FM ordering, which coincides with the temperature of the metal-insulator transition, a, b, c - are the unit cell parameters at room temperature for the Pnma setting. The compositions with $y = 0.75$ (O-18), $y = 0.9$ and $y = 1$ are insulators down to helium temperatures. For the compositions with $y \geq 0.6$, the AFM ordering is observed together with the ferromagnetic ordering, and $T_{AFM} \approx$ const. ≈ 150 K.

Sample	y	$\langle r_A \rangle$, Å	t	T_{FM}, K	a, Å	b, Å	c, Å	Comment
	0	1.206	0.9207	250	5.4654	7.7231	5.4798	from [23]
	0.25	1.199	0.9181	~ 200	5.4585	7.7146	5.4674	from [22]
LPCM-50	0.5	1.193	0.9160	175	5.4616	7.7080	5.4591	
LPCM-60	0.6	1.190	0.9149	150	5.4587	7.6987	5.4540	
LPCM-70	0.7	1.187	0.9138	130	5.4609	7.6940	5.4480	
LPCM-75	0.75	1.186	0.9134	120	5.4566	7.6929	5.4479	O-16
LPCM-75	0.75	1.186	0.9134	–	5.4567	7.6932	5.4479	O-18
LPCM-80	0.80	1.185	0.9130	100	5.4663	7.6907	5.4443	
LPCM-90	0.90	1.182	0.9119	95	5.4641	7.6895	5.4420	
LPCM-100	1.00	1.179	0.9109	80	5.4674	7.6856	5.4382	
	1	1.179	0.9109	120	5.4646	7.6749	5.4308	from [22]

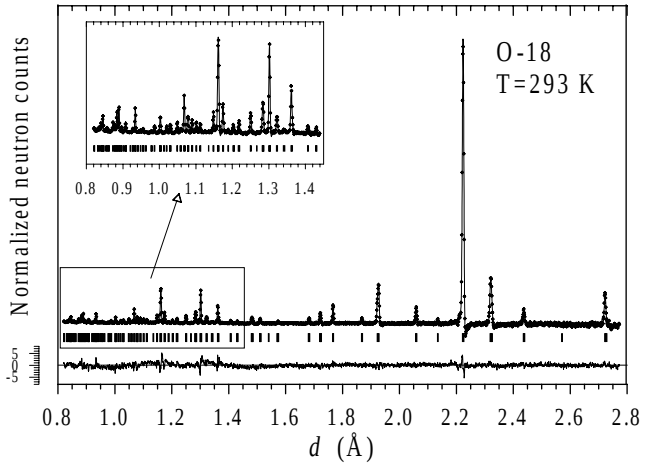

Fig. 1. Diffraction spectrum of the LPCM-75 (O-18) sample, measured at the HRFD at room temperature and treated with Rietveld method. The experimental points, calculated profile and difference curve are shown. The difference is weighted by the mean-squares deviation for each point. Ticks below the graph indicate the calculated peak positions.

All structural data are given for the orthorhombic space group Pnma (No. 62) in the standard setting, for which the unit cell parameters are related to that of the ideal cubic perovskite ($a_c \approx 3.8$ Å) by the formulae: $a \approx c \approx \sqrt{2}\, a_c$, $b \approx 2a_c$.

The structural neutron-diffraction experiments were carried out with the HRFD diffractometer in the FLNP, JINR at the IBR-2 pulsed reactor. HRFD is the TOF correlation neutron spectrometer utilising the fast Fourier-chopper for modulation of the neutron beam intensity and the reverse time-of-flight method for registration of scattered neutrons [20]. The resolution of HRFD in the interplanar distance d_{hkl} scale is defined by the maximal chopper rotation speed and only slightly depends on d_{hkl}. In the experiments with LPCM, $\Delta d/d$ was near 0.0015, which allowed to obtain the precise structural information. In particular, the statistic errors of the unit cell parameters determination were less than 10^{-4} Å, and for the interatomic distances they did not exceed 0.002 Å. The diffraction spectra were measured in the regime of heating the samples from helium to room temperatures. Correspondingly, the values of the phase transition temperatures are given for this particular regime. For Rietveld refinements, the MRIA program [21] was used; they were normally done in the d_{hkl} interval from 0.8 to 2.8 Å. An example of the diffraction spectrum measured at the HRFD and treated with Rietveld method, is given in Figure 1.

3 $(La_{1-y}Pr_y)_{0.7}Ca_{0.3}MnO_3$ crystal structure

3.1 Room temperature structure

The results obtained in the present paper for the $(La_{1-y}Pr_y)_{0.7}Ca_{0.3}MnO_3$ with $y = 0.5-1.0$, together with the earlier published structural parameters of LPCM with $y = 0.25$ and 1.0 [22] and $y = 0$ [23], allow us to analyse the structure as a function of the average A-cation radius. According to the already stated tradition (see, for example, Ref. [22]), as the parameter for such an analysis we use the values tabulated in reference [24] for the nine-fold coordination of cation. Assuming, according to reference [24], $r_{La} = 1.217$ Å, $r_{Pr} = 1.179$ Å and $r_{Ca} = 1.180$ Å, we get, that increasing of y in LPCM from 0 to 1 leads to the decrease in $\langle r_A \rangle$ from 1.206 to 1.179 Å. The extreme values of $\langle r_A \rangle$ correspond to the low-temperature metallic and insulating states of LPCM, and the composition with $y \approx 0.75$ is situated on the border between them.

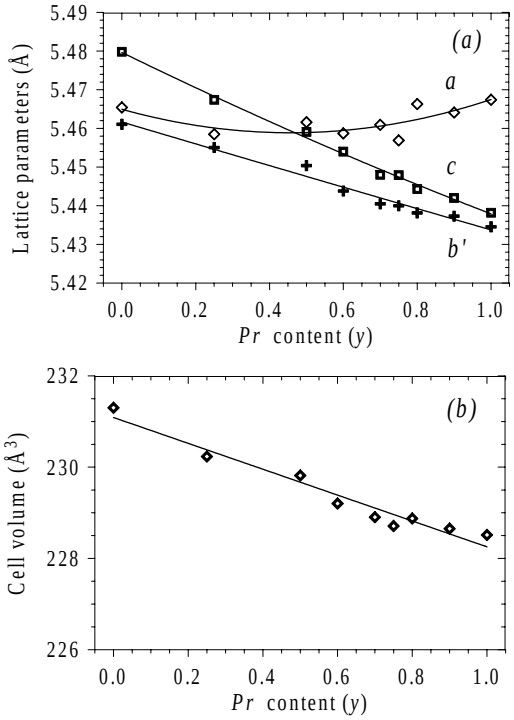

Fig. 2. Dependencies of the unit cell parameters (a) of $(La_{1-y}Pr_y)_{0.7}Ca_{0.3}MnO_3$ ($b' = b/\sqrt{2}$) and its volume (b) at room temperature on the Pr content. The points for $y = 0$ and 0.25 are taken from references [23] and [22], correspondingly. The lines through the points for the unit cell parameters are the guides for the eye. The unit cell volume dependence on the Pr content was fitted with linear function. The experimental errors of the points are smaller than the symbol sizes.

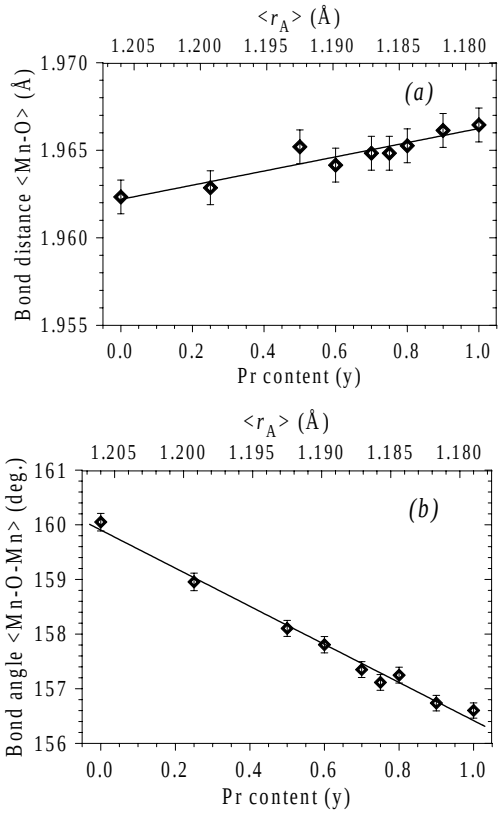

Fig. 3. Dependencies of the average values for the ⟨Mn-O⟩ bond length (a) and the ⟨Mn-O-Mn⟩ valence angle (b) at room temperature on the Pr content. The points for $y = 0$ and 0.25 are taken from literature (Refs. [23] and [22]). Linear fits were obtained by the least-squares method. At the upper x-axis, the calculated average A-cation ionic radii corresponding to the particular Pr content values are presented.

The dependencies of the LPCM unit cell parameters and volume on the Pr content are shown in Figure 2.

They are monotonic, and the decrease of the unit cell volume with increasing Pr content is linear. The dependencies of the average values of the Mn-O distance and Mn-O-Mn angle on $\langle r_A \rangle$, shown in Figure 3, are practically linear.

The change of the angle in the extreme points is quite significant (about 2.5%), while the ⟨Mn-O⟩ distance is changing by not more than 0.15%.

The conducting bandwidth W, which defines the FM-transition temperature in manganites ($T_{FM} \propto W$), is directly connected to the valence angle: $W \propto \cos\varphi$, where $\varphi = [\pi - \langle \text{Mn-O-Mn} \rangle]$ [25]. Figure 4 shows T_{FM} for the LPCM compositions undergoing the FM-transition as a function of the average valence angle ⟨Mn-O-Mn⟩. T_{FM} is in fact a linear function of ⟨Mn-O-Mn⟩ (it does not matter which variable is used: the angle or its cosine since the angle is only slightly changing), implying that the average Mn-O-Mn angle is the main structural parameter governing the electronic properties.

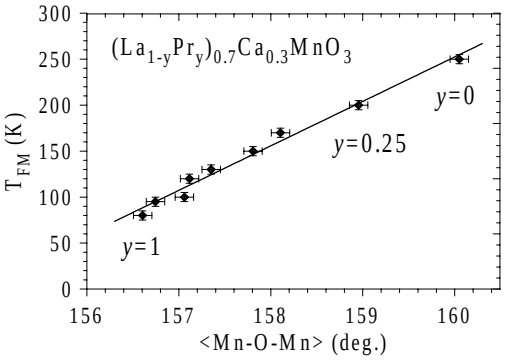

Fig. 4. The onset temperature T_{FM} of the long-range FM order in the series of $(La_{1-y}Pr_y)_{0.7}Ca_{0.3}MnO_3$ compounds as a function of the average value of the Mn-O-Mn valence angle. Solid line is linear fit to the data. Data for $y = 0$ and 0.25 compositions are taken from references [23] and [22].

3.2 Temperature behavior of structural parameters

For all the compositions, the unit cell parameters dependencies on temperature have quite a complicated character, which reflects the changes of the atomic and magnetic structure in them (see Fig. 5 as an example).

The most typical peculiarities are the decreasing of the a and b parameters below the transition to the FM phase and the characteristic minimum in the b-parameter temperature dependence near 180 K (practically absent for $y = 0.5$ and very weak for $y = 0.6$), which might

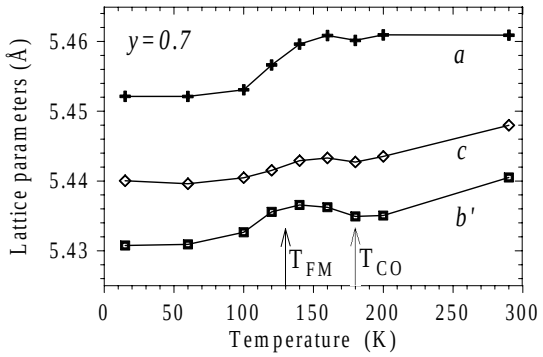

Fig. 5. Temperature dependencies of a, b, and c ($b' = b/\sqrt{2}$) unit cell parameters for the LPCM-70. The temperatures of CO and FM transitions are marked with arrows. The lines drawn through the experimental points are guides for the eye. The symbol sizes are larger than the experimental errors.

be connected to the beginning of the charge ordering process [8]. The transition to the AFM state, which is observed for the compositions with $y \geq 0.70$, is not revealed in the unit cell parameters behaviour. To complete the picture, in Figure 6 the comparison of the unit cell parameters behavior for the LPCM-75 compositions with O-16 and O-18 isotopes is shown.

One can see that the unit cell parameters of these two samples are changing identically, moreover, their absolute values practically coincide above the transition of the O-16 sample to the metallic phase. This fact may be considered as justification of the initial structural identity of the O-16 and O-18 samples, in particular, with respect to the oxygen content with high precision (for details see Ref. [12]). The unit cell volume undergoes a jump-like decrease at the transition to the metallic ferromagnetic state in all studied compositions, except for the O-18 sample, which remains insulating in the whole temperature range. The value of this jump-like decrease of volume only slightly depends on y, and amounts to about 0.15%.

At room temperature the oxygen octahedra in LPCM-50 compound are almost regular, *i.e.* all three independent bonds, Mn-O1 (along the b axis), Mn-O21 and Mn-O22 (in the a-c plane) have practically equal lengths. While approaching the temperature of the phase transition into the metallic FM state, the strong octahedra distortion appears. The Jahn-Teller parameter of the octahedra distortion

$$\sigma_{\mathrm{JT}} = \sqrt{1/3 \sum [(\mathrm{Mn\text{-}O})_i - \langle \mathrm{Mn\text{-}O} \rangle]^2},$$

is about 9.1×10^{-3} Å at $T = 200$ K. This value is ~ 2 times larger, than, for example, the maximal distortion of the octahedra in the $La_{0.75}Ca_{0.25}MnO_3$ compound [22]. Upon reaching the saturated FM state, (at $T \approx 150$ K) the "melting" of the orbital ordering occurs and the bond lengths become equal again. For the LPCM-60 and LPCM-70 compositions, the changes of the bond lengths are less pronounced, but in the temperature dependencies of the average values the peculiarity is clearly observed at T_{FM}. In Figure 7, the temperature dependencies of the

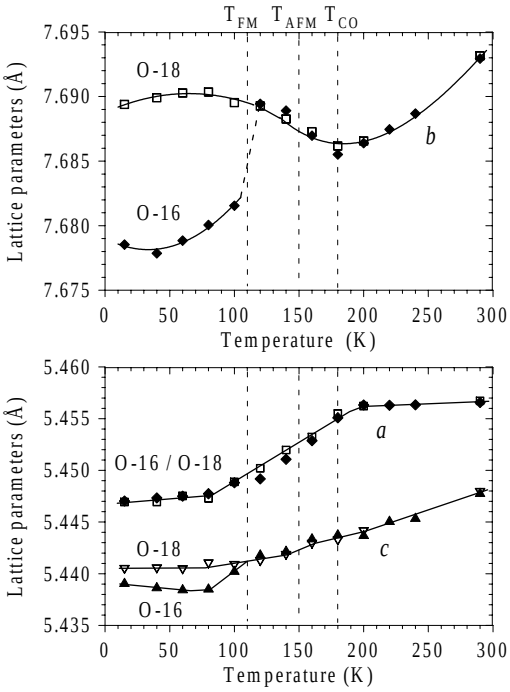

Fig. 6. Temperature dependencies of the unit cell parameters for the O-16 (solid symbols) and O-18 (open symbols) samples of LPCM-75. Between T_{FM} and room temperature all three parameters are practically coinciding in the both samples. The identity of a parameters is preserved in the whole temperature range. The vertical lines mark the temperatures of CO, AFM and FM transitions. The lines drawn through the experimental points are guides for the eye. The symbol sizes are larger than the experimental errors.

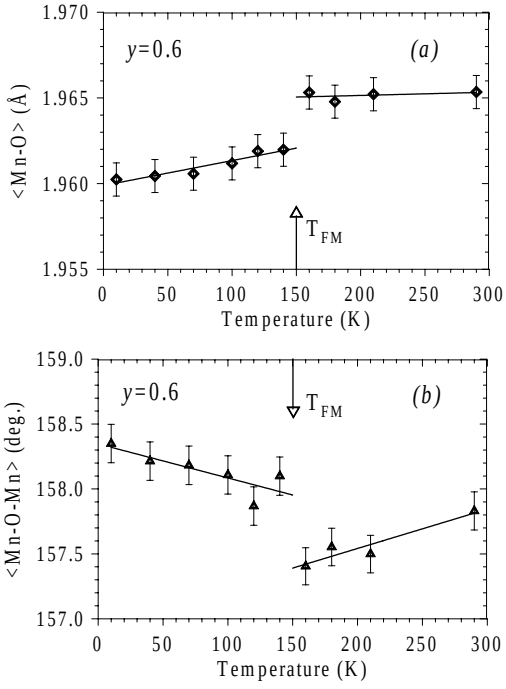

Fig. 7. Temperature dependencies of the average Mn-O bond length (a) and of the average Mn-O-Mn valence angle (b) for LPCM-60 compound. Arrows indicate the temperature of the transition into the FM state.

Table 2. Lattice parameters, coordinates of atoms, Mn-O bond lengths, and Mn-O-Mn bond angles in $(La_{0.25}Pr_{0.75})_{0.7}Ca_{0.3}MnO_3$ at $T = 293$ K and $T = 15$ K for samples with ^{16}O and ^{18}O isotopes (O-16 and O-18 samples). Mn thermal parameter was fixed at 0.4 Å^2 (for $T = 293$ K) and at 0.2 Å^2 (for $T = 15$ K), O1 and O2 thermal parameters were equalized.

	$T = 293$ K			$T = 15$ K		
Parameter	O-16	O-18	Difference	O-16	O-18	Difference
a, Å	5.45657(7)	5.45673(6)	−0.00016(10)	5.44805(7)	5.44797(6)	−0.00008(10)
b, Å	7.69294(9)	7.69315(8)	−0.00021(12)	7.67918(9)	7.69054(8)	−0.01136(12)
c, Å	5.44788(8)	5.44786(7)	0.00002(11)	5.43869(8)	5.43945(7)	0.00076(11)
La (x)	0.0290(3)	0.0276(4)		0.0320(3)	0.0337(4)	
La (z)	−0.0013(8)	−0.0017(8)		−0.0116(8)	−0.0111(8)	
La (B), Å^2	0.31(3)	0.49(3)		0.2	0.2	
O1 (x)	0.4884(5)	0.4905(4)		0.4894(5)	0.4890(4)	
O1 (z)	0.0718(4)	0.0722(4)		0.0717(4)	0.0750(4)	
O2 (x)	0.2840(3)	0.2852(3)		0.2824(3)	0.2834(3)	
O2 (y)	0.0369(2)	0.0366(2)		0.0362(2)	0.0370(2)	
O2 (z)	0.7174(3)	0.7180(3)		0.7168(3)	0.7193(3)	
O (B), Å^2	0.63(3)	0.54(3)		0.39(3)	0.42(3)	
Mn-O1, Å	1.965(1)	1.965(1)	0.000(1)	1.960(1)	1.966(1)	−0.006(1)
Mn-O21, Å	1.959(2)	1.951(2)	0.007(3)	1.958(2)	1.972(2)	−0.014(3)
Mn-O22, Å	1.971(2)	1.978(2)	0.007(3)	1.964(2)	1.950(2)	0.014(3)
⟨Mn-O⟩, Å	1.9648	1.9646	0.0002(10)	1.960	1.963	−0.003(1)
Mn-O1, Å	1.965(1)	1.965(1)	0.000(1)	1.960(1)	1.966(1)	−0.006(1)
Mn-O21, Å	1.959(2)	1.951(2)	0.007(3)	1.958(2)	1.972(2)	−0.014(3)
Mn-O22, Å	1.971(2)	1.978(2)	0.007(3)	1.964(2)	1.950(2)	0.014(3)
⟨Mn-O⟩, Å	1.9648	1.9646	0.0002(10)	1.960	1.963	−0.003(1)
Mn-O1-Mn, deg.	156.43(5)	156.38(5)	0.05(7)	156.79(5)	155.78(5)	1.01(7)
Mn-O2-Mn, deg.	157.8(2)	157.8(2)	0.00(3)	157.9(2)	157.9(2)	0.0(2)
⟨Mn-O-Mn⟩, deg.	157.12	157.11	0.01(5)	157.35	156.83	0.52(5)

⟨Mn-O⟩ and ⟨Mn-O-Mn⟩ values for LPCM-60 are shown. The typical abrupt jumps in ⟨Mn-O-Mn⟩ angle and in ⟨Mn-O⟩ distance are clearly seen at $T = T_{FM}$. The similar dependencies are observed in the other compositions as well. More detailed analysis shows that the jump in lattice parameters at T_{FM} is equally due to the jump-like change of distances and angles both in the (a, c) plane, and along the b axis.

3.3 Comparative structural analysis of ^{16}O and ^{18}O enriched samples

The room and low temperature structural parameters of the LPCM-75 samples with ^{16}O and ^{18}O isotopes obtained from Rietveld refinements are presented in Table 2.

In the O-18 sample, which remains insulating down to helium temperature, they are weakly changing with temperature, the Jahn-Teller distortion of the octahedra is significant, $\sigma_{JT} \approx 12 \times 10^{-3}$ Å at $T = 200$ K and only slightly decreases with temperature lowering down to 15 K. In the O-16 sample, the Mn-O bond lengths coincide within the experimental error bars with that in O-18 down to 110 K, however, upon reaching the saturated FM state at $T_S \approx 80$ K in this sample, the structurally non-equivalent Mn-O bond lengths converge to the mean value. The differences in the structural behaviour of O-16 and O-18 samples are clearly seen in Figures 8 and 9, where the temperature dependencies of the Mn-O bond lengths and of the Mn-O-Mn valence angles are shown, both in-plane and along b-axis. Both in-plane average ⟨Mn-O2⟩ bond length and in-plane Mn-O2-Mn valence angle behave identically in the O-16 and O-18 samples within the accuracy of experimental data in the whole temperature range. On the contrary, along b-axis, there is a pronounced difference between both the values of Mn-O1-Mn angle and of Mn-O1 bond length in them below $T_{FM,O\text{-}16}$ (110 K). It is obvious that at $T \approx 110$ K in the O-16 sample, the abrupt changes (same as in LPCM-60) of the Mn-O1 bond length (by ~ 0.003 Å) and of the Mn-O1-Mn valence angle (by $\sim 0.7°$) occur, while in the O-18 sample these values remain practically constant. Decrease of Mn-O1 in O-16 is the main reason for the jump in b parameter, and, as a consequence, in the unit cell volume.

It is worth mentioning that the structural analysis of the perovskite compound $PrNiO_3$ [26], in which the large shift of the Néel temperature $T_N = T_{I\text{-}M}$ (by ~ 10 K)

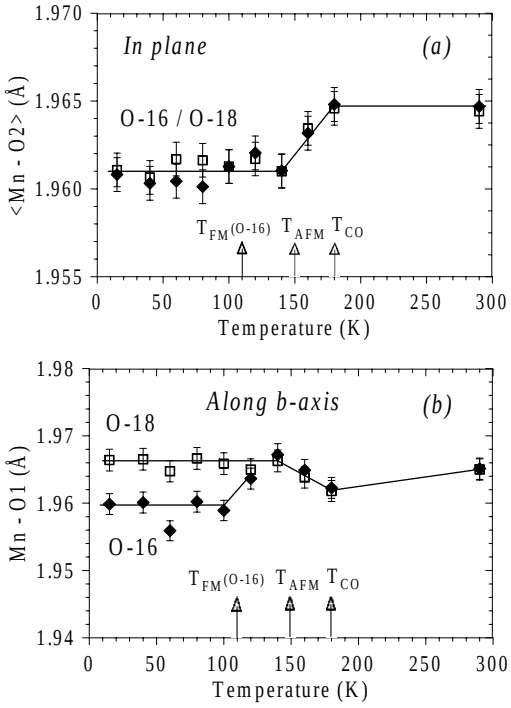

Fig. 8. Comparison of the temperature dependencies of the average of in plane Mn-O2 bond lengths (a) and of the Mn-O1 bond length along *b*-axis (b) for the O-16 and O-18 samples (shown, correspondingly, by closed and opened symbols) of LPCM-75 composition. Arrows indicate the temperatures of the phase transitions into the CO, AFM (for both samples), and FM (for O-16 sample) states.

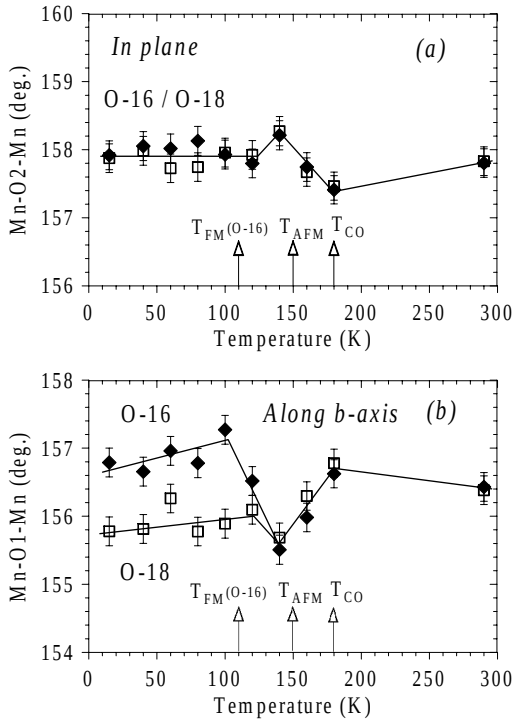

Fig. 9. Comparison of the temperature dependencies of the Mn-O2-Mn (a) and Mn-O1-Mn (b) valence angles for the O-16 and O-18 samples (shown, correspondingly, by closed and opened symbols) of LPCM-75 composition. Arrows indicate the temperatures of the phase transitions into the CO, AFM (for both samples), and FM (for O-16 sample) states.

caused by ^{16}O for ^{18}O substitution was observed, has also shown the sudden changes in the ⟨Ni-O⟩ bond length (by ~ 0.004 Å) and ⟨Ni-O-Ni⟩ angle (by $\sim 0.8°$) at a metal-insulator transition point. However, ⟨Ni-O⟩ and ⟨Ni-O-Ni⟩ behaved identically in the samples with ^{16}O and ^{18}O. Such a comparison confirms that the difference in the structural parameters of O-16 and O-18 samples below 110 K reflects the difference in their magnetic and transport properties in this temperature region.

4 Phase separation at onset of the FM state in O-16 sample

The distinctive temperature behaviour of the FM and AFM diffraction peak intensities in LPCM-80 sample is shown in Figure 10. The same synchronism in the temperature dependencies of the diffraction peaks intensities, connected with the Mn-cations charge and AFM ordering with typical maximum near $T_{\rm FM}$ for the O-16 sample of LPCM-75 was observed earlier [12]. As it was pointed out in reference [12], this behaviour may be naturally explained in the two-phase model. Namely, with the temperature decrease, the charge ordering of the structure occurs ($T_{\rm CO} \approx 180$ K), which serves as the background for the collinear AFM ordering appearance, at $T_{\rm AFM} \approx 150$ K. At further temperature decrease, and approaching the

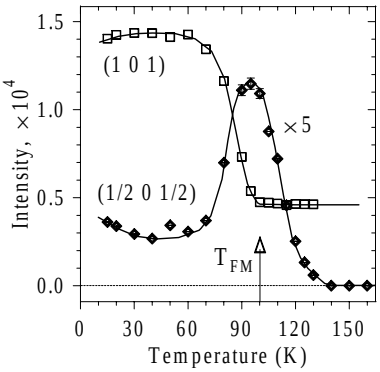

Fig. 10. Temperature dependencies of the FM (1 0 1) and AFM (1/2 0 1/2) diffraction peak intensities of the LPCM-80 sample. The (1/2 0 1/2) peak intensities were multiplied by a factor of 5. Where not shown, the error bars are smaller than the symbol sizes. The lines are guides for the eye. At $T = 100$ K, the long-range FM order appears and the sample passes on to the two phase (AFM ($\sim 20\%$) + FM ($\sim 80\%$)) state.

$T_{\rm FM} \approx 110$ K, the clusters of the ferromagnetic phase start to grow inside the antiferromagnetic matrix similar to those registered by the small-angle [27] or by the magnetic diffuse neutron scattering [28]. Appearance of the metallic FM state is accompanied by the percolative phase transition (its theoretical basis is given, for example, in Ref. [29]), resulting in the onset of the long-range FM order in the major part of the sample volume.

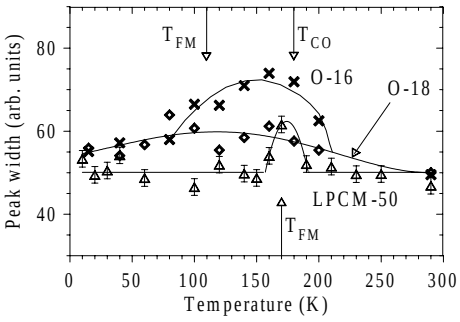

Fig. 11. Temperature dependencies of the diffraction peak widths for the LPCM-50 and LPCM-75 (O-16 and O-18) samples. The arrows indicate the temperatures of FM transitions in LPCM-50 (in the bottom) and O-16 (in the top), and also the onset temperature of the charge ordering process in O-16.

In this scenario, the broadening of the diffraction peaks should be one of the observed effects. It may be caused by the appearance of microstresses in the crystal matrix with formation of the FM phase, or by the low dimensions of the coherently scattering regions. This broadening is actually observed, if the experiment is carried out at the diffractometer with high resolution. For example, in reference [8] while investigating the $Pr_{0.7}Ca_{0.3}MnO_3$ composition, the authors observed significant peak broadening starting from the temperature $\sim$ 30 K above the FM transition, and the peaks remained broadened down to helium temperature.

The LPCM compositions investigated in the present paper have the quasi-cubic lattice with very close unit cell parameters and despite the high resolution of the HRFD diffractometer, at which the atomic structure was defined, the spectra do not have completely isolated diffraction peaks. Hence, the widths of the diffraction peaks were defined in the Rietveld structure refinements. In Figure 11, the temperature dependencies of the diffraction peak width of the LPCM-50 and LPCM-75 samples with ^{16}O and ^{18}O isotopes are presented. It is seen that, both at room, and at helium temperature the peak widths of these samples are approximately equal. In the LPCM-50 sample (which undergoes the FM transition at $\sim$ 170 K, and at $\sim$ 150 K the metallic FM state in it is already close to the saturation), the peak width is practically constant in the whole temperature range, except for the narrow region between 160 and 190 K, where it significantly increases (by $\sim$ 20%). In the O-16 sample (with $y = 0.75$), the peak width increases by $\sim$ 15% in the range from $\sim$ 180 K, where the charge ordering process begins, down to $\sim$ 80 K, where the transition into the metallic saturated FM phase finishes. In the O-18 sample, which remains insulating in the whole temperature range, the peak width does not change.

The strong overlapping of the diffraction peaks and non-linear change of the unit cell parameters with temperature do not allow to carry out more quantitative analysis of the observed peak broadening effects. In our case it is impossible to separate the broadening effects caused by the microstresses from that conditioned by the small sizes of the magnetically ordered regions. We can only conclude that in the O-16 sample, unlike in the O-18 one, in the temperature region 80–180 K (below T_{CO}), the strongly inhomogeneous state exists.

5 Discussion and conclusions

In this article, some new results of the neutron-diffraction structural investigation of $(La_{1-y}Pr_y)_{0.7}Ca_{0.3}MnO_3$ compositions in the wide temperature and Pr-concentration y ranges are presented. Their analysis together with the data obtained earlier allows revealing of the correlation between the transport and microscopic properties of these perovskite manganites. As in the other CMR perovskites, the relation between $\langle r_A \rangle$ and atomic structure can be seen in LPCM. Decrease of $\langle r_A \rangle$ from 1.206 to 1.179 Å leads to the linear decrease of the mean $\langle$Mn-O-Mn$\rangle$ valence angle (by 2.5% in total) and to the increase of the average $\langle$Mn-O$\rangle$ distance (by 0.15%). This turns out to be enough for changing of the metallic state of LPCM to the insulating and for changing of the magnetic state from pure ferromagnetic to the mixed FM+AFM one. Lowering of the mean $\langle$Mn-O-Mn$\rangle$ valence angle results in approximately linear decrease in the conduction bandwidth, which correspondingly causes the linear decrease of T_{FM}. At the same time, since conditions for the appearance of AFM structure are mainly defined by the superexchange between localized Mn-spins, T_{AFM} temperature remains approximately constant ($T_{AFM} \approx 150$ K in LPCM) and the AFM order disappears, if T_{FM} exceeds T_{AFM}. In the proximity of the phase boundary between metallic and insulating states (close to $y \approx 0.7$, $\langle$Mn-O-Mn$\rangle \approx 157°$), the two-phase state appears at low temperatures, which is especially sensitive to the different influences, including oxygen isotope substitution.

The characteristic "melting" of the distorted oxygen octahedra at the transition to the ferromagnetic metallic phase is more clearly observed for the composition with $y = 0.5$. For this composition, $T_{FM} = 175$ K is considerably higher than $T_{AFM} = 150$ K, at which the antiferromagnetic ordering may occur in LPCM compounds 30% doped by calcium. The average values of the Mn-O distance and Mn-O-Mn angle have abrupt changes at T_{FM}, which are manifested in the temperature dependencies of the unit cell parameters and volume.

The data obtained for the ^{16}O and ^{18}O enriched compositions with $y = 0.75$ have shown the structural identity of these two samples in the interval between the room temperature and the temperature of the ^{16}O composition transition into the FM metallic phase. Below $T_{FM,O\text{-}16} = 110$ K, the statistically significant differences in the average values of the bond lengths and valence angles of Mn and O in the O-16 and O-18 samples have been registered. However, the comparison of the structural parameters in the compositions undergoing the I-M transition ($y = 0.5 - 0.8$) with the composition $y = 1$, which remains insulating, shows that the observed differences are due to the transition of the O-16 sample into

the ferromagnetic metallic state and, consequently, the different low-temperature state of the O-16 and O-18 samples below $T_{FM,O\text{-}16}$ is only caused by the different dynamics of the oxygen atoms.

The observed changes in the diffraction peaks widths at temperatures above the saturated FM state, and also the synchronism of the changes of the diffraction peaks intensities, characteristic for the CO and AFM states of the O-16 and O-18 samples, are the clear arguments in favor of the theoretical models, suggesting that the FM-metallic states arising at low temperatures are inhomogeneous. The phase transition into this state has probably the percolation character with appearance of the FM clusters in the insulating matrix, their subsequent growth and fusion, resulting in the appearance of the long-range FM order and the metallic conductivity.

It is well known that the size of the charge separated regions is regulated by the Coulomb energy and cannot be large ("foggy" state). The sharp diffraction lines which we do see from both FM- and AFM-CO-phases mean that the size of these regions is large, according to our estimation not less than 1000 Å, *i.e.* pure electronic phase separation [30] is not realized in this compound. The same conclusion was made in the recent paper of Uehara *et al.* [31], where the size of the separated regions was estimated by electron microscopy data as large as several thousands ångströms. In the comments to Uehara *et al.* paper, Littlewood [32] proposed "strain fields in random orientation" as a factor which can stabilize the non-uniform FM- and AFM-CO-state. Our structural data for O-16 and O-18 samples of $(La_{0.25}Pr_{0.75})_{0.7}Ca_{0.3}MnO_3$ can be regarded as a direct evidence that interatomic distances and bond angles are different in the coexisting metallic and insulating phases. Thus, the long-range phase separation process in the $(La_{1-y}Pr_y)_{0.7}Ca_{0.3}MnO_3$ manganites has structural nature.

The authors are grateful to V.G. Simkin and A.V. Pole for their help in carrying out the neutron-diffraction experiment at the HRFD. We are also thankful to V.A. Amelichev, A.A. Bosak, E.A. Chistotina, A.V. Inyushkin and A.N. Taldenkov for their help in the samples preparation and their characterization. The work has been done with the help of the RFBR program (project 00-02-16736) and of the INTAS-RFBR foundation (projects IR-97-1954, I-97-0963).

References

1. G.M. Zhao, K. Conder, H. Keller, K.A. Muller, Nature (London) **381**, 676 (1996).
2. G.M. Zhao, H. Keller, J. Hofer, A. Shengelaya, K.A. Muller, Sol. St. Comm. **104**, 57 (1997).
3. N.A. Babushkina, L.M. Belova, O.Yu. Gorbenko, A.R. Kaul, A.A. Bosak, V.I. Ozhogin, K.I. Kugel, Nature (London) **391**, 159 (1998).
4. G.H. Jonker, J.H. Van Santen, Physica (Amsterdam) **16**, 337 (1950).
5. P. Schiffer, A.P. Ramirez, W. Bao, S.-W. Cheong, Phys. Rev. Lett. **75**, 3336 (1995).
6. Z. Jirak, S. Krupicka, Z. Simsa, M. Dlouha, S. Vratislav, J. Magn. Magn. Mater. **53**, 153 (1985).
7. H. Yoshizawa, H. Kawano, Y. Tomioka, Y. Tokura, Phys. Rev. B **52**, R13145 (1995)
8. D.E. Cox, P.G. Radaelli, M. Marezio, S.-W. Cheong, Phys. Rev. B **57**, 3305 (1998).
9. H.Y. Hwang, S.-W. Cheong, P.G. Radaelli, M. Marezio, B. Batlogg, Phys. Rev. Lett. **75**, 914 (1995).
10. N.A. Babushkina, L.M. Belova, V.I. Ozhogin, O.Yu. Gorbenko, A.R. Kaul, A.A. Bosak, D.I. Khomskii, K.I. Kugel, J. Appl. Phys. **83**, 7369 (1998).
11. A.M. Balagurov, V.Yu. Pomjakushin, V.L. Aksenov, N.M. Plakida, N.A. Babushkina, L.M. Belova, O.Yu. Gorbenko, A.R. Kaul, P. Fischer, M. Gutmann, L. Keller, JETP Lett. **67**, 705 (1998).
12. A.M. Balagurov, V.Yu. Pomjakushin, D.V. Sheptyakov, V.L. Aksenov, N.A. Babushkina, L.M. Belova, A.H. Taldenkov, A.V. Inyushkin, O.Yu. Gorbenko, A.R. Kaul, P. Fischer, M. Gutmann, L. Keller, Phys. Rev. B **60**, 383 (1999).
13. M.R. Ibarra, G.M. Zhao, J.M. De Teresa, B. García-Landa, Z. Arnold, C. Marquina, P.A. Algarabel, H. Keller, C. Ritter, Phys. Rev. B **57**, 7446 (1998).
14. A.J. Millis, P.B. Littlewood, B.I. Shraiman, Phys. Rev. Lett. **74**, 5144 (1995).
15. A.J. Millis, B.I. Shraiman, R. Mueller, Phys. Rev. Lett. **77**, 175 (1996).
16. E.O. Wollan, W.C. Koehler, Phys. Rev. **100**, 545 (1955).
17. D.N. Argyriou, J.F. Mitchell, C.D. Potter, D.G. Hinks, J.D. Jorgensen, S.D. Bader, Phys. Rev. Lett. **76**, 3826 (1996).
18. J.L. García-Muñoz, M. Suaaidi, J. Fontcuberta, J. Rodriguez-Carvajal, Phys. Rev. B **55**, 34 (1997).
19. E.L. Nagaev, Phys. Rev. B **58**, 12242 (1998).
20. V.L. Aksenov, A.M. Balagurov, V.G. Simkin, A.P. Bulkin, V.A. Kudryashev, V.A. Trounov, O. Antson, P. Hiismaki, A. Tiitta, J. Neutron Research **5**, 181 (1997).
21. V.B. Zlokazov, V.V. Chernyshev, J. Appl. Cryst. **25**, 591 (1992).
22. P.G. Radaelli, G. Iannone, M. Marezio, H.Y. Hwang, S.-W. Cheong, J.D. Jorgensen, D.N. Argyriou, Phys. Rev. B **56**, 8265 (1997).
23. Q. Huang, A. Santoro, J.W. Lynn, R.W. Erwin, J.A. Borchers, J.L. Peng, K. Ghosh, R.L. Greene, Phys. Rev. B **58**, 2684 (1998).
24. R.D. Shannon, Acta Cryst. A **32**, 751 (1976).
25. J.B. Goodenough, J. Appl. Phys. **81**, 5330 (1997).
26. M. Medarde, P. Lacorre, K. Conder, J. Rodriguez-Carvajal, S. Rosenkranz, F. Fauth, A. Furrer, Physica B **241-243**, 751 (1998)
27. J.M. De Teresa, M.R. Ibarra, P.A. Algarabel, C. Ritter, C. Marquina, J. Blasco, J. García, A. del Moral, Z. Arnold, Nature **386**, 256 (1997).
28. P.G. Radaelli, G. Iannone, D.E. Cox, M. Marezio, H.Y. Hwang, S.-W. Cheong, Physica B **241**, 295 (1998).
29. L.P. Gor'kov, Physics-Uspekhi **41**, 589 (1998).
30. E.L. Nagaev, Physics-Uspekhi **39**, 781 (1996).
31. M. Uehara, S. Mori, C.H. Chen, S.-W. Cheong, Nature (London) **399**, 560 (1999).
32. P. Littlewood, Nature (London) **399**, 529 (1999).